Highlights of Spanish Astrophysics VI, Proceedings of the IX Scientific Meeting of the Spanish Astronomical Society held on September 13 - 17, 2010, in Madrid, Spain. M. R. Zapatero Osorio et al. (eds.)

Physical properties of Hα selected star forming galaxies at $z \sim 0.84$

Víctor Villar[1], Jesús Gallego[1], Pablo G. Pérez-González[1,2], Guillermo Barro[1], Sergio Pascual[1], Jaime Zamorano[1], Kai Noeske[3], and David Koo[3]

[1] Departamento de Astrofísica, Facultad de CC. Físicas, ,Universidad Complutense de Madrid, E-28040 Madrid, Spain
[2] Associate Astronomer at Steward Observatory, The University of Arizona, 933 N Cherry Avenue, Tucson, AZ 85721, USA
[3] Lick Observatory, University of California, Santa Cruz, CA 95064

Abstract

In this work we analyze the star formation rates and stellar masses of a sample of 157 star forming galaxies at $z \sim 0.84$ [5], selected by their Hα flux with a narrow band filter. We compare star formation rates (SFR) measured with different tracers (Hα, UV and IR) finding that they are in good agreement after extinction correction, although with some scatter. We find a correlation between the ratios $\mathrm{SFR_{FUV}/SFR_{H\alpha}}$, $\mathrm{SFR_{IR}/SFR_{H\alpha}}$ and the EW(Hα) (i.e. weighted age) which accounts for part of this scatter. We obtained stellar mass estimations fitting templates to multi-wavelength photometry. The typical stellar mass of a galaxy within our sample is $\sim 2 \times 10^{10}$ $\mathrm{M_\odot}$. The specific star formation rate (sSFR) decreases with it, indicating that massive galaxies are less affected by star formation processes than less massive ones. In addition, the sSFR is, for a fixed mass, higher in the Universe at $z \sim 0.84$ than in the local one. Both results are consistent with the *downsizing* scenario. To quantify this *downsizing* we estimated the *quenching* masses for our sample at $z \sim 0.84$ and a local sample also selected by Hα, finding that it declines from $M_\mathrm{Q} \sim 10^{12}$ $\mathrm{M_\odot}$ at $z \sim 0.84$ to $M_\mathrm{Q} \sim 8 \times 10^{10}$ $\mathrm{M_\odot}$ at the local Universe.

1 Introduction

In this work we use a narrow band selected sample of star forming galaxies at $z \sim 0.84$, presented in [5] (hereafter V08), to compare SFRs obtained from different tracers and to study the relation between stellar mass and SFR. The sample is very well suited for this study as: i) it is directly selected by star formation, thus we are not biasing the population of

star forming galaxies, and ii) the use of the narrow band filter technique provides us reliable Hα SFRs to compare with FUV and IR estimations.

2 Sample

This paper analyzes an Hα selected sample of galaxies at $z = 0.84$. The objects are selected by their emission in the Hα+[NII] line and are thus selected due to intense star formation (except when activity at nuclei level is present). The sample was first described in V08 and the reader is referred to that paper for full details on the sample selection criteria. A brief summary of the process is presented here.

The sample was built using narrow and broad band images in the J band of the near infrared. The narrow-band filter used in this work is J-continuum ($J_{\rm C}$) centered at 1.20 μm, corresponding to Hα at $z = 0.84$. The search was performed using the near-infrared camera OMEGA-2000 on the 3.5 m telescope at CAHA. Three pointings were observed, two in the EGS and another one in the GOODS-North field, covering a whole area of ~ 0.174 deg^2, and reaching 70% completeness at a line flux of $\sim 1.5 \times 10^{-16}$ erg s^{-1} cm^{-2}.

In a first step, 239 emission line candidates were selected (once excluded the stars) by their flux excess in the narrow band, showing a $J - J_{\rm C}$ colour excess significance $n_\sigma > 2.5$ in one or several apertures. Spectroscopic and photometric redshifts were then used to rule out contaminants, either emission line galaxies at other redshifts or objects selected by strange spectral features or noise. First, the sample was cross-checked against redshift catalogs on GOODS-N and EGS fields. A total of 76 objects were confirmed as genuine Hα emitters in the narrow band redshift range, 43 in the Extended Groth Strip and 33 in GOODS-N. Contaminants were mainly emission line galaxies at other redshifts and a few objects not selected by line emission. The accuracy selecting emission line galaxies was very high, around $\sim 90\,\%$. Spectroscopic redshifts were only available for 98 objects in the sample, therefore photometric redshifts were used to get rid of interlopers for the rest of the sample. Considering the photometric redshifts, a total of 89 objects, 64 in the EGS and 25 in GOODS-N, were added to the final sample.

The final sample of Hα emitters at $z = 0.84$ contains 165 objects, 107 in the EGS and 58 in GOODS-N, 79 (48 %) of them confirmed by optical spectroscopy (after including three objects with low quality spectroscopic redshift). However, due to insufficient complementary data for some objects we have discarded 8 objects. Hence, the sample used in this paper is composed of 157 objects.

3 Hα luminosity function

The Hα luminosity function was calculated applying the $V/V_{\rm max}$ method:

$$\phi(\log L_i) = \frac{1}{\Delta \log L} \sum_j \frac{1}{V(z)_j}, \qquad (1)$$

where L_i is the central luminosity in the bin i and $V(z)_j$ is the maximum volume in which object j can be detected.

Before computing the Hα luminosity function we have to consider two important effects affecting our sample: extinction and completeness.

The amount of extinction for each galaxy was estimated through the FIR to UV flux ratio or through the UV slope when the FIR data was not available (see V08). The median extinction is 1.5 mag in Hα, adopting values between 0 and 4 mag. Once applied these corrections, Hα luminosities and star formation rates were computed.

In order to determine the limiting flux and completeness corrections we carried out simulations. The limiting fluxes vary from field to field from 8×10^{-17} erg s^{-1} cm^{-2} to 14×10^{-17} erg s^{-1} cm^{-2} for a 70 % completeness level. The completeness correction depends on the line flux and was applied to the LF in order to obtain its real shape.

The LF can be seen in Fig. 1. The resulting best fit to a Schechter function gives (V08):

$$\begin{aligned} \phi^* &= 10^{-2.76\pm0.32}\,\mathrm{Mpc}^{-3} \\ L^* &= 10^{42.97\pm0.27}\,\mathrm{erg\ s}^{-1} \\ \alpha &= -1.34 \pm 0.18 \end{aligned} \tag{2}$$

In the fitting process, we discarded the faintest and the brightest bins. The faintest bin was clearly affected by incompleteness. The brightest bin fell off the general shape of the best Schechter fit. Moreover, it contains only one object, which could be there due to a wrong estimation of the reddening or a photo-z outlier. Figure 1 shows the extinction-corrected LF derived in this work as well as in [1], [4] and [3] corrected for extinction LFs. [4] applied an overall extinction correction $A_V = 1$ mag obtained from the CFRS sample, except for two galaxies where high quality spectra were available and $f(\mathrm{H}\beta)$ and $f(\mathrm{H}\delta)$ could be measured. [1] did not attempt the extinction correction though we can apply the typical correction $A(\mathrm{H}\alpha) = 1$ mag [2] for these kind of surveys. [3] used the same selection technique, based in this work, though they applied a mean extinction correction instead of a individual one. This results in very different shapes between the LFs, although the selection technique is the same.

The SFRd derived from the extinction corrected LF is $\dot{\rho}_* = 0.17^{+0.03}_{-0.03}$ M$_\odot$ yr^{-1} Mpc^{-3}. The strong increase from $z = 0$ to $z \sim 1$ found in other surveys is confirmed. Combining just the Hα-based SFR densities obtained by our group from $z = 0.02$, $z = 0.24$, $z = 0.40$ and $z = 0.84$ Hα-selected samples, we obtain an evolution of the cosmic SFR density $\propto (1+z)^\beta$ where $\beta = 3.8 \pm 0.5$.

4 Star formation rates

This work uses the Hα luminosity as the principal estimator of the instantaneous SFR of galaxies. The Hα line flux has been used to select the sample, making it very suitable to study star formation processes, as it has been selected by this property. However, star formation involves physical processes whose imprint become observable along a wide range

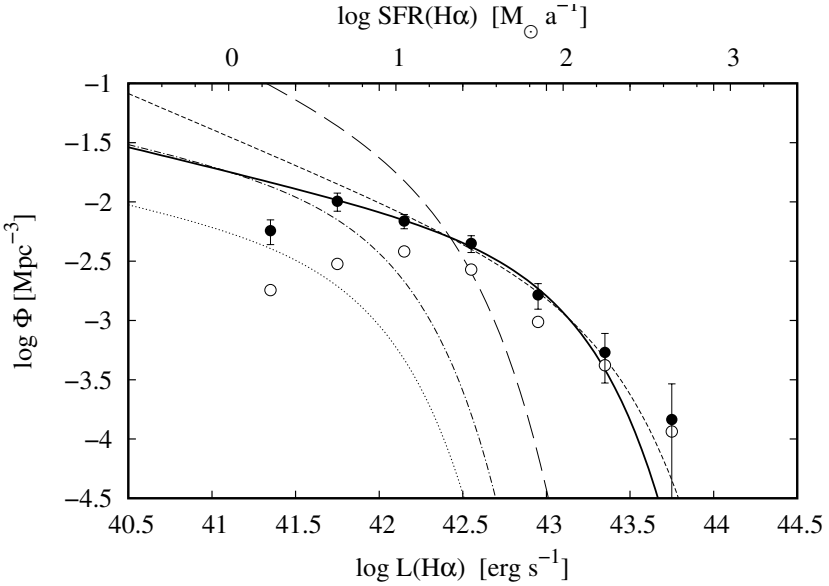

Figure 1: Hα luminosity function (filled circles) with the best fit to a Schechter function (thick line). the open circles show the LF before applying the completeness correction. We also show the star forming galaxies Hα LF (dotted line), as well as the [1] (dashed line), [4] (dotted-dashed line) and [3] (long dashed line).

of the electromagnetic spectrum: X-rays, ultraviolet, forbidden recombination lines ([O II]), far infrared, radio, etc. In this work, in addition to Hα, given the depth and coverage of the multi wavelength data available, we estimate SFRs through far ultraviolet and far infrared luminosities. Each tracer is affected by different phenomenons and is originated by different physical mechanisms, related (at least in part) with star formation processes. Thus, the different results obtained with different tracers could yield some information about the properties of the galaxy that hosts the star formation processes.

The comparison between Hα and FUV star formation rates is plotted in Fig. 2. Estimations coming from both tracers now agree within a factor of 3: $\langle \mathrm{SFR_{FUV}} \rangle = 15^{+30}_{-10}$ $\mathrm{M_\odot\ yr^{-1}}$, $\langle \mathrm{SFR_{H\alpha}} \rangle = 13^{+27}_{-9}$ $\mathrm{M_\odot\ yr^{-1}}$. The good agreement corroborates that our extinction corrections are working well and that these galaxies do not host star forming regions totally attenuated in the UV but visible in Hα, at least globally.

In the case of the IR we find $\langle \mathrm{SFR_{H\alpha}} \rangle = 27^{+45}_{-19}$ $\mathrm{M_\odot\ yr^{-1}}$, which is 30% lower than the IR derived value $\langle \mathrm{SFR_{IR}} \rangle = 36^{+65}_{-23}$ $\mathrm{M_\odot\ yr^{-1}}$. However, this value leads to confusion, as a few outliers contaminate the value. If we work with the ratios of SFRs we find that Hα provides slightly lower estimates ($\langle \mathrm{SFR_{IR}/SFR_{H\alpha}} \rangle = 1.1$), but in agreement with IR estimates within uncertainties.

The scatter between the different tracers ($\mathrm{SFR_{FUV}/SFR_{H\alpha}}$, $\mathrm{SFR_{IR}/SFR_{H\alpha}}$) are correlated with the Hα equivalent width. This can be explained through the different weighted age of the objects (which is related to the EW) and the fact that FUV and IR SFRs are

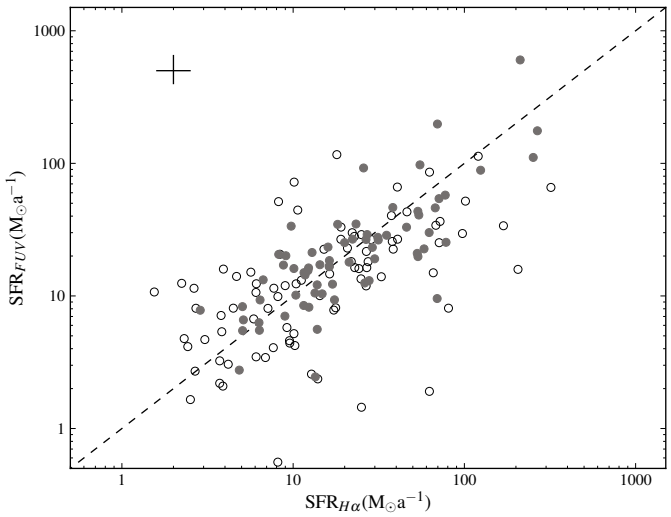

Figure 2: Comparison of SFRs inferred from Hα luminosity and FUV luminosity.

sensitive to a longer time range than Hα, being more affected by older populations.

5 Stellar masses

The estimate of stellar mass is obtained from the best fitting template to the SED of each galaxy. The template provides mass-to-light ratios for each observed band and a stellar mass is computed for each one. The final value is the average of the values obtained for each observed band, being the associated error the standard deviation of the distribution of stellar masses.

The median and standard deviation for the distribution are $M_\star = 1.6^{+5.2}_{-1.3} \times 10^{10}$ M$_\odot$. The typical mass of an star-forming galaxy (to the limit of our sample) is ten times lower than the typical mass of the global population of galaxies.

There exists an anti-correlation between the sSFR (SFR per unit of stellar mass) and the stellar mass, evidencing that star formation processes have a higher impact on less massive galaxies. This trend is also present in the star forming galaxies of the local Universe, with a similar slope in the case of the UCM sample, although shifted in the sSFR axis to lower values, indicating that the star formation is less important (see Fig. 3).

The star formation mass relation holds up until a certain mass, above which it no longer holds and the star formation drops sharply. Galaxies above this mass are considered quiescent, as star formation processes are no longer the main drivers of its evolution and they move to the red sequence.

With our data it is possible to estimate an upper limit for ths *quenching* mass. For the sake of clarity we are going to use the *doubling* time t_d, which is analogous to the sSFR. In

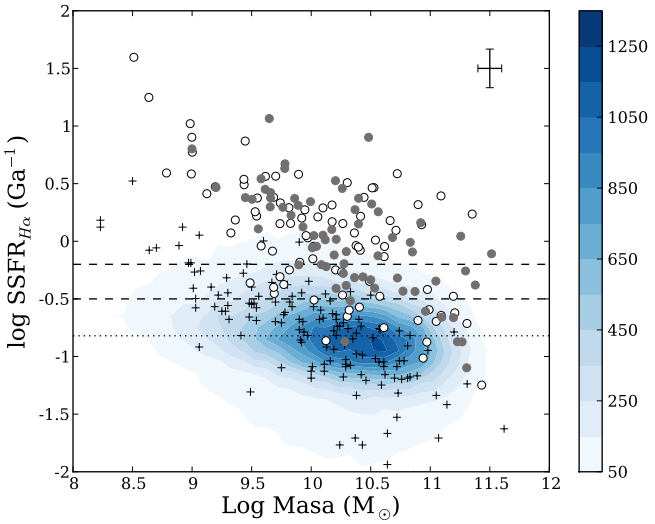

Figure 3: Specific SFR versus stellar mass. Filled and open circles represent the sample at $z = 0.84$. The crosses stand for the UCM local sample of star forming galaxies and the blue colormap represents the SDSS local sample.

order to estimate the *quenching* mass we define a galaxy as quiescent if its *doubling* time is higher than what we define as *quenching* time: $t_{\rm Q} = 3 \times t_{\rm H}$, where $t_{\rm H}$ is the Hubble time.

We obtain that $M_{\rm Q} = 1.3^{+1.3}_{-0.6} \times 10^{12}$ M$_\odot$ ($\log(M_{\rm Q}/{\rm M}_\odot) = 12.1 \pm 0.3$) for the $z \sim 0.84$ sample and $M_{\rm Q} = 7.9^{+1.9}_{-1.5} \times 10^{10}$ M$_\odot$ ($\log(M_{\rm Q}/{\rm M}_\odot) = 10.9 \pm 0.1$) for the local sample. The *quenching* mass evolves by an order of magnitude from the Local universe to that at $z = 0.84$.

References

[1] Hopkins, A. M., Connolly, A. J., & Szalay, A. S. 2000, AJ, 120, 2843

[2] Pascual, S., Gallego, J., & Zamorano, J. 2007, PASP, 119, 30

[3] Sobral, D., Best, P. N., Geach, J. E., Smail, I., Kurk, J., Cirasuolo, M., Casali, M., Ivison, R. J., Coppin, K., & Dalton, G. B. 2009, MNRAS, 398, 75

[4] Tresse, L., Maddox, S. J., Le Fèvre, O., & Cuby, J.-G. 2002, MNRAS, 337, 369

[5] Villar, V., Gallego, J., Pérez-González, P. G., Pascual, S., Noeske, K., Koo, D. C., Barro, G., & Zamorano, J. 2008, ApJ, 607, 169 (V08)